Available online at www.sciencedirect.com
SCIENCE DIRECT®
Polymer 45 (2004) 2453–2464
polymer
www.elsevier.com/locate/polymer

Concentration dependence of viscometric properties of model short chain polymer solutions

T. Kairn, P.J. Daivis*, M.L. Matin, I.K. Snook

Department of Applied Physics, RMIT University, GPO Box 2476V, Melbourne, Victoria 3001, Australia

Received 25 July 2003; received in revised form 10 December 2003; accepted 11 December 2003

Abstract

We study the concentration dependence of the conformational and viscometric behaviour of short-chain polymer solutions in shear flow by conducting a series of non-equilibrium molecular dynamics simulations, covering the entire concentration range. Our model explicitly incorporates all of the important generic features of real polymer solutions—excluded volume, hydrodynamic interactions and finite chain extensibility. Hydrodynamic interactions are included exactly by treating the solvent explicitly as an atomic fluid. The polymer molecules studied consist of 20-site bead-rod model molecules, which correspond approximately to 12 Kuhn steps in the melt. For polyethylene, this represents a molar mass of 1800 g mol^{-1}. In some respects, our results are consistent with experimental and theoretical results obtained for long-chain polymer solutions. We calculate the Flory–Fox constant and find a value that agrees reasonably well with results for long chain polymer solutions. Due to the short chain length of the molecules investigated, no semidilute region exists for these solutions. However, the radius of gyration and viscosity still exhibit strong concentration dependence, which is well described by power series, rather than power law expressions, in contrast to the behaviour usually observed in long-chain polymer solutions.

PACS: 82.35. − x; 83.60. − a; 66.20. + d

Keywords: Shear flow; Bead rod model polymer; Non-equilibrium molecular dynamics

1. Introduction

Our understanding of the static and dynamic properties of polymer solutions is based on the successful theoretical description provided by scaling and renormalization group theories [1–3], the Rouse and Zimm models of polymer dynamics, the concepts of static and hydrodynamic screening and the Doi–Edwards tube model for molecular motion in the presence of entanglements [4]. During the past few decades, these models have been subjected to intense scrutiny using a wide variety of experimental and computational techniques. As a result of these investigations, we now have a rather complete picture of the types of polymer fluids that are well-described by these theories. Generally, the description applies best to very high molecular weight polymers in athermal solvents either in the limit of infinite dilution, or above the overlap concentration. Less attention seems to have been given to the transition from dilute to moderately concentrated solutions or the transition from oligomeric to polymeric solutions. When the standard description fails to describe experimental data, discrepancies are often attributed to the chains being too short, the solvent quality being too poor or other complicating factors such as chain branching, polydispersity or specific chemical interactions [5].

Computer simulation studies of polymer solutions make it possible to eliminate some of these complicating factors. The polydispersity and branching of model polymers studied in computer simulations are exactly specified by the model (and usually absent), and the solvent quality is also easily modified, but other limitations are imposed by currently available computational speed. In particular, the chain lengths studied in computer simulations are generally quite small, even when compared to the smallest values commonly used in experimental studies, and the representation of the solvent is sometimes severely simplified in order to achieve computational speed. Nevertheless, the polymer solutions studied in molecular dynamics computer simulations where both polymer and solvent are represented

* Corresponding author. Tel.: +61-3-99253393; fax: +61-3-99255290.
E-mail address: peter.daivis@rmit.edu.au (P.J. Daivis).

0032-3861/$ - see front matter © 2003 Elsevier Ltd. All rights reserved.
doi:10.1016/j.polymer.2003.12.034

explicitly, are generally regarded as being relatively realistic and there have been many cases in which theories of polymer behaviour have been verified by molecular dynamics simulations of short-chain polymer solutions.

For example, the dynamics of a dilute polymer solution (actually a single chain in explicit solvent with periodic boundary conditions) has been investigated, using molecular dynamics simulations, by Dunweg and Kremer [6] and Pierleoni and Ryckaert [7], who found that the predictions of the Zimm model were essentially confirmed for polymer chains with maximum degree of polymerization $N = 60$ and $N = 30$ in the respective studies. More recently, Ahlrichs, Everaers and Dunweg [8] used molecular dynamics simulations in combination with a coarse-grained lattice-Boltzmann model of the solvent to investigate the dynamics of semidilute polymer solutions ($N = 1000$) and found evidence supporting the idea of hydrodynamic screening, but only on length and time scales that are large enough for topological constraints to become effective. This is consistent with the picture introduced by de Gennes, now generally agreed to be at least qualitatively correct in the long chain limit.

However, many instances remain in which the properties of polymer fluids are not adequately described by theory. These instances are important, because by understanding them better, we will be better able to model real polymer solutions in which the molecular weight is regarded as too small for the application of scaling and renormalization-group theories and the tube model.

Two deficiencies stand out. First, it was remarked in 1975 by Daoud et al. [9] that the mechanism for the change in the radius of gyration of a polymer molecule at concentrations lower than the critical overlap concentration is poorly understood. This remains true today, and it is shown later that this mechanism is particularly important for short-chain polymer solutions. Second, there is no adequate theoretical prediction of the concentration dependence of viscosity for short-chain polymer solutions. The low-concentration limit is usually described in terms of the Zimm model and the Huggins expansion, and the high concentration limit is usually described using the modified Rouse model, but there is apparently no single theory that links these two limits [4]. This contrasts with the description based on scaling, screening and reptation, which, at least qualitatively describes the concentration dependence of the viscosity for high molecular weight polymer solutions above the overlap concentration. A complete theory of polymer rheology should capture the transition from Zimm and Huggins behaviour to either Rouse or reptation dynamics as the concentration is increased. We hope that, by investigating the transition from Huggins to Rouse behaviour, we will obtain a clearer physical understanding of the various mechanisms that collectively determine the concentration dependence of the viscosity for real polymer solutions.

In this article, we report the results of equilibrium and non-equilibrium molecular dynamics simulations of short-chain polymer solutions in a good solvent, covering the entire concentration range. Conformational properties such as the mean squared radius of gyration and mean squared end-to-end distance, and viscometric properties such as the viscosity and first and second normal stress coefficients, are studied as a function of concentration. The concentration dependence of these quantities is discussed in the context of standard polymer solution theory. We compute the solution viscosity as a function of concentration, and obtain the intrinsic viscosity and Huggins coefficient for this model polymer solution, which can be superficially compared with experimental results. We also use the intrinsic viscosity to calculate a value for the Flory–Fox parameter, Φ. This parameter can be compared more reliably with the results of experiment and theory because its asymptotic value is independent of polymer molar mass.

2. Molecular model and simulation technique

2.1. Molecular model

The molecular dynamics approach treats all particles in the system, including solvent molecules, explicitly. In the work described here, the solvent molecules are modelled as spherical Lennard–Jones particles, while the polymer molecules are modelled as 20-site chains of similar spheres. The polymer molecules are represented by a bead-rod model with truncated and shifted Lennard–Jones (LJ) interactions between all beads ('sites') except those which are bonded to each other within a molecule.

The potential energy function describing all interactions (polymer–polymer, polymer–solvent and solvent–solvent) is given by

$$\phi(r_{ij}) = \begin{cases} 4\epsilon\left[\left(\dfrac{\sigma}{r_{ij}}\right)^{12} - \left(\dfrac{\sigma}{r_{ij}}\right)^{6}\right] - \phi_c, & r_{ij} \le r_c \\ 0, & r_{ij} > r_c \end{cases} \quad (1)$$

where r_{ij} is the separation of two interaction sites, ϵ is the potential well depth and σ is the value of r_{ij} at which the unshifted potential is zero. The shift, ϕ_c, which is equal to the value of the unshifted potential at the cutoff $r_{ij} = r_c$, is introduced to eliminate the discontinuity in the potential energy. At distances greater than the cutoff distance r_c, the potential is zero. For this set of simulations, we have taken the cutoff point for the potential to be the position of the minimum in the LJ potential, $r_c = 2^{1/6}\sigma$. An LJ potential with this truncation point is often known as the WCA potential [10], and it results in purely repulsive interactions. This potential is convenient for computational work because it is short-ranged, and therefore computationally undemanding, but still retains the essential physics, i.e. the repulsive (excluded volume) interaction.

All interaction sites have equal mass $m_{i\alpha} = m$ and the

bonds between polymer interaction sites have length $l = \sigma$. This bond length is chosen to be small enough to prevent chain crossings.

In the remainder of this paper, we express all quantities in terms of site reduced units for which the reduction parameters are the site–site Lennard–Jones interaction parameters ϵ and σ and the mass m of each site.

2.2. Equations of motion

Planar shear flow (PSF) in the x direction with velocity gradient in the y direction can be described by the velocity gradient tensor $\nabla\mathbf{u}$, given by

$$\nabla\mathbf{u} = \begin{bmatrix} 0 & 0 & 0 \\ \dot{\gamma} & 0 & 0 \\ 0 & 0 & 0 \end{bmatrix} \tag{2}$$

where $\dot{\gamma}$ describes the rate of strain. For the low shear rates used in this study, certain viscometric and conformational parameters are expected to be linearly related to even powers of the strain rate. Therefore, in this study, results are illustrated relative to $\dot{\gamma}^2$, rather than simply $\dot{\gamma}$.

We use the molecular version of the well-established SLLOD equations of motion [11–15], which are given by

$$\dot{\mathbf{r}}_{i\alpha} = \frac{\mathbf{p}_{i\alpha}}{m_{i\alpha}} + \mathbf{r}_i \cdot \nabla\mathbf{u} \tag{3}$$

$$\dot{\mathbf{p}}_{i\alpha} = \mathbf{F}^{\mathrm{LJ}}_{i\alpha} + \mathbf{F}^{\mathrm{C}}_{i\alpha} - \frac{m_{i\alpha}}{M_i}\mathbf{p}_i \cdot \nabla\mathbf{u} - \zeta^{\mathrm{M}}\frac{m_{i\alpha}}{M_i}\mathbf{p}_i \tag{4}$$

where $\mathbf{r}_{i\alpha}$ and $\mathbf{p}_{i\alpha}$ represent the position and thermal momentum of site α of molecule i, $\mathbf{r}_i$ represents the position of the centre of mass of molecule i, $m_{i\alpha}$ is the mass of site $i\alpha$ $\mathbf{F}^{\mathrm{LJ}}_{i\alpha}$ represents the sum of all LJ type forces on site α of molecule i and $\mathbf{F}^{\mathrm{C}}_{i\alpha}$ represents the sum of all bond length constraint forces on site α of molecule i. ζ^{M} is the thermostat multiplier, given by

$$\zeta^{\mathrm{M}} = \frac{\sum_{i=1}^{N_{\mathrm{m}}} (\mathbf{F}_i \cdot \mathbf{p}_i - \mathbf{p}_i \cdot \nabla\mathbf{u} \cdot \mathbf{p}_i)/M_i}{\sum_{i=1}^{N_{\mathrm{m}}} \mathbf{p}_i^2/M_i} \tag{5}$$

where $\mathbf{p}_i = \sum \mathbf{p}_{i\alpha}$ represents the centre of mass momentum of molecule i, M_i is the mass of molecule i, $\mathbf{F}_i$ is the total force on molecule i, and N_{m} is the number of molecules in the system. This expression for ζ^{M} is derived from Gauss' principle of least constraint, and acts to keep the molecular centre of mass kinetic temperature T^{M} constant, rather than the atomic or site temperature. T^{M} is defined by

$$T^{\mathrm{M}} = \frac{1}{k_{\mathrm{B}} f} \sum_{i=1}^{N_{\mathrm{m}}} \frac{\mathbf{p}_i^2}{M_i} \tag{6}$$

where f represents the number of translational centre of mass degrees of freedom, which depends on the total number of sites and the number of constraints (holonomic and non-holonomic) on the system. The details of this algorithm, including its statistical mechanical basis, the constraint algorithm, and the thermostat, have been discussed previously [11–15].

Note that in the equations of motion, the same strain rate and thermostat terms are applied to all sites on a given molecule. This means that they only affect the centre of mass degrees of freedom and cannot interfere with intramolecular (particularly the rotational) degrees of freedom. Alternative forms of the equations of motion and thermostating terms can be applied, but they can result in a non-zero antisymmetric stress and artificially enhanced orientational ordering. These issues have also been discussed in detail previously [16–19]. For our current purposes, the molecular centre of mass thermostat will suffice, since the reduced strain rates used are well below $\dot{\gamma} = 1.0$, where all thermostats give identical results.

2.3. Viscometric functions

The pressure tensor was calculated using the molecular expression

$$\mathbf{P}V = \left\langle \sum_{i=1}^{N_{\mathrm{m}}} \frac{\mathbf{p}_i \mathbf{p}_i}{M_i} - \frac{1}{2}\sum_{i=1}^{N_{\mathrm{m}}}\sum_{\alpha=1}^{N}\sum_{j\neq 1}^{N_{\mathrm{m}}}\sum_{\beta=1}^{N} \mathbf{r}_{ij}\mathbf{F}^{\mathrm{inter}}_{i\alpha j\beta} \right\rangle \tag{7}$$

where, as before, $\mathbf{p}_i$ represents the total thermal momentum of molecule i, $\mathbf{r}_{ij}$ is the separation of the centres of mass of molecules i and j, and $\mathbf{F}^{\mathrm{inter}}_{i\alpha j\beta}$ represents the intermolecular force on site $i\alpha$ due to site $j\beta$. For solvent molecules, the number of sites per molecule is equal to one, and for pure solvent, the molecular pressure tensor reduces to the usual atomic expression.

In the presence of a non-equilibrium flow field, the non-equilibrium component of the pressure tensor is given by

$$\mathbf{\Pi} = \mathbf{P} - p_0\mathbf{1} \tag{8}$$

where p_0 is the equilibrium pressure, equal to one third of the trace of the equilibrium pressure tensor ((1/3)Tr($\mathbf{P}_0$)). It is also useful to define a total pressure $p = (1/3)\mathrm{Tr}(\mathbf{P})$ so that the change in the pressure with strain rate is given by

$$\Delta p = p - p_0. \tag{9}$$

It is now well established that both the pressure and the internal energy are observed to vary strongly with strain rate in NEMD simulations [11–14]. This occurs because the strain rates that are easily studied by NEMD are of order 1 in reduced units, which corresponds to approximately 10^{12} s^{-1} for liquid Argon or 10^{11} s^{-1} for CH_4, in real units. In this work, the strain rates used are unusually low for NEMD simulations (being no greater than 0.0022 in reduced units) and are comparable to the strain rates used in a recent direct comparison between experiment and simulation [20]. At these strain rates, we find that values of Δp are very small; most are zero within errors.

The viscometric functions of the system are defined by components of the pressure tensor $\mathbf{P}$. For our shear flow geometry, defined by Eq. (2), the generalized non-Newtonian shear viscosity of a fluid subject to PSF is defined as:

$$\eta_s = -\frac{P_{xy} + P_{yx}}{2\dot{\gamma}}. \tag{10}$$

The two normal stress differences are

$$N_1 = P_{yy} - P_{xx} \tag{11}$$

and

$$N_2 = P_{zz} - P_{yy}. \tag{12}$$

These result from restoring forces which act in opposition to any flow-induced anisotropy in the fluid and can be used to calculate the corresponding normal stress coefficients

$$\Psi_1 = \frac{P_{yy} - P_{xx}}{\dot{\gamma}^2} \tag{13}$$

and

$$\Psi_2 = \frac{P_{zz} - P_{yy}}{\dot{\gamma}^2}. \tag{14}$$

Experimentally, the first normal stress coefficient, Ψ_1, is observed to approach a constant value as shear rate approaches zero, while Ψ_2 has been found to be of the order $-(1/10)\Psi_1$ [21]. For simple shear flow, η_s, Ψ_1 and Ψ_2 are useful material functions for representing and relating the three independent components of the stress tensor. They are examined in detail in Section 3.2.

2.4. Simulation details

The equations of motion given above are solved at each time-step by a five-value Gear predictor–corrector scheme with a time-step of 0.004 reduced time units. Bulk behaviour is simulated via periodic boundary conditions (PBCs) and the minimum image convention, which prescribes that the simulation box must be sufficiently large and the range of the interaction sufficiently short that each particle interacts only with the closest image of any other particle.

Our algorithm for constant (N, V, T^M) simulations of solutions of Lennard–Jones chain molecules undergoing shear flow is based on the Evans, Edberg and Morriss algorithm [13–15], which we have substantially modified to simulate planar elongational flow [22–25]. The current study extends the work of Matin, Daivis and Todd who simulated homogeneous shear and elongational flow in chain molecular fluids with degree of polymerization $N =$ 1, 2 and 4 [24] and later $N = 2$, 4, 10, 20 and 50 [26,27]. However, in this article, we only report the results of planar shear flow simulations.

The polymer site fraction, n_1, is defined as the fraction of sites in the system which belong to polymer molecules. This quantity is used henceforward to describe the concentration of the systems. Table 1 lists the values of n_1 and the polymer mass concentrations (mass of polymer per unit volume of solution) in the solutions studied here, calculated from the relation $\rho_1 = n_1\rho$, where ρ is the overall mass density of the solution which remains fixed at 0.84 in reduced units for all of our simulations. This differs slightly from the usual experimental situation, in which the pressure remains fixed and small changes in volume due to mixing are possible. We expect only minor differences between the results obtained by varying the concentration at constant total density or constant pressure. However, this is something that should be investigated in future work.

The interaction between a given site and its own periodic image is an unwanted and unphysical artefact of molecular simulations that may occur due to the use of periodic boundary conditions (PBCs). In the case of direct interactions, this artefact is avoided by truncating the potential and choosing the box size to be sufficiently large. Hydrodynamic interactions, which are forces between polymer segments propagated by flow of the suspension medium, can have a sufficiently long range to seriously affect simulations of dilute polymer solutions in periodic boundary conditions [6]. We have determined that the solutions used in this study are of sufficiently high concentration that hydrodynamic interactions have substantially decayed over the distance between periodic images. We have used large systems, with a total number of sites (solvent atoms plus polymer sites) of 10,000, to ensure that our periodic box is large enough to allow the decay of long-range hydrodynamic interactions, as well as to give suitably accurate statistics. Through the simulation of a smaller system with only 5120 sites, we were able to establish (as reported in Section 3.2) that PBC-related artifacts had no detectable effect on our results.

The various polymer and solvent systems used in these simulations were generated from a single 20-site polymer melt. Relevant proportions of the polymer chain molecules in this system were broken into single-site molecules, by simply changing the way they were defined in the program, to produce the six different concentrations desired. Each of the systems thus produced was then equilibrated for at least

Table 1
Simulation parameters: total number of sites (N_s), number of polymer molecules (N_m), polymer site fraction (n_1) and reduced polymer mass concentration (ρ_1). Parameters in square brackets are used only in Section 3.2

N_s	N_m	n_1	ρ_1
10,000	0	0.0	0.000
10,000	100	0.2	0.168
[5120]	[51]	[0.2]	[0.167]
10,000	200	0.4	0.336
10,000	300	0.6	0.504
10,000	400	0.8	0.672
10,000	500	1.0	0.840

4,000,000 time-steps, at each of the six required shear rates ($\dot{\gamma} = 0.0000$, 0.0005, 0.00071, 0.0010, 0.0016 and 0.0022) to ensure that a steady state had been reached. Thereafter, a production run of 4,000,000 time-steps was completed for each of the 36 systems.

During each of these production runs, properties of the system were calculated every 0.1 reduced time units, with these being averaged into 10 or 20 blocks for the production runs, enabling the calculation of standard errors in the means of all measured properties [24]. Conformational data quoted in Section 3.1 were averaged over every polymer molecule in the simulation box for five instantaneous states at each concentration.

3. Results and discussion

3.1. Polymer conformation

Polymer molecules in dilute solutions are typically separated from one another and coiled up to occupy an elliptical region with a continually varying shape and orientation [28], so that the time-averaged polymer conformation in the laboratory coordinate system forms a sphere with a size defined by the radius of gyration, R_g

$$R_g^2 = \frac{1}{2N^2} \sum_i \sum_j \langle r_{ij}^2 \rangle \tag{15}$$

where N is the number of sites in the chain and r_{ij} is the distance between sites i and j on the molecule. The magnitude of R_g depends on the quality of the solvent in which the polymer is suspended. The relationship between the spatial distance between two sites and the number of bonds between the two sites is given by $\langle r_{ij}^2 \rangle \propto |j - i|^{2\nu}$ where ν, the Flory exponent, depends on solvent quality. For poor solvents, where the chains behave ideally and can be described by Gaussian random walk statistics, ν is equal to 0.5 (so that $\langle r_{ij}^2 \rangle \propto |j - i|$). In good solvents, however, polymer chains exhibit excluded volume effects and swell so that the molecule executes a self-avoiding walk and ν is greater than 0.5. Flory's mean field theory predicts that ν in a good solvent should be 0.6 [29] whereas more precise renormalization group theory and numerical computation gives a value of 0.588 [1,2].

Experimental studies have shown that properties such as the radius of gyration and osmotic pressure undergo a marked change in behavior as the concentration increases and the domains occupied by different molecules begin to overlap, but this change occurs gradually—not at a precise value of concentration. For sufficiently high molecular weight molecules, there exists a semi-dilute concentration regime where the polymer chains overlap, but their overall volume fraction remains low. The existence of a semi-dilute regime requires the existence of a length scale ξ such that $b_K \ll \xi \ll R$, where b_K is the Kuhn length and R is the equilibrium root mean square end-to-end distance. In this regime, the average concentration of the solution is comparable to the local concentration within the domain of each molecule. Theoretical predictions of the concentration dependence of the solution properties in the semidilute regime are available [1,2,4]. These properties are also expected to depend upon the strain rate in a shearing system.

The following results are presented as an exploration of these theoretical issues. Here, we examine the concentration and shear rate dependence of the polymer size in terms of the mean squared radius of gyration and the mean squared end-to-end distance. Fig. 1 shows the behaviour of $R_{g,s}^2$, the shear rate dependent mean squared radius of gyration of the polymer molecules, with respect to $\dot{\gamma}^2$ for each of the different concentrations simulated (excluding $n_1 = 0.0$). The linear behaviour of the data in this figure allows us to define the zero-shear rate mean squared radius of gyration, R_g^2, of the polymers in each solution using the relationship

$$R_{g,s}^2 = a\dot{\gamma}^2 + R_g^2 \tag{16}$$

where a, calculated as the gradient of $R_{g,s}^2$ versus $\dot{\gamma}^2$, obviously varies with polymer concentration. Values of a and R_g^2 for our systems are listed in Table 2. Clearly, polymer size increases with increasing shear rate at all concentrations, though this phenomenon becomes less pronounced as polymer concentration is decreased (as shown by the drop in a with decreasing n_1 in Table 2). Evidently, the polymer molecules in the more dilute solutions are in a swollen state at equilibrium, so the shear flow can have little effect on their size. Conversely, those polymer molecules which are unperturbed at zero shear rate are liable to be stretched more by the effect of shear. Overall, polymer size decreases with increasing concentration for all of the shear rates used here, so that polymers in concentrated solutions never find themselves as expanded as their dilute solution counterparts.

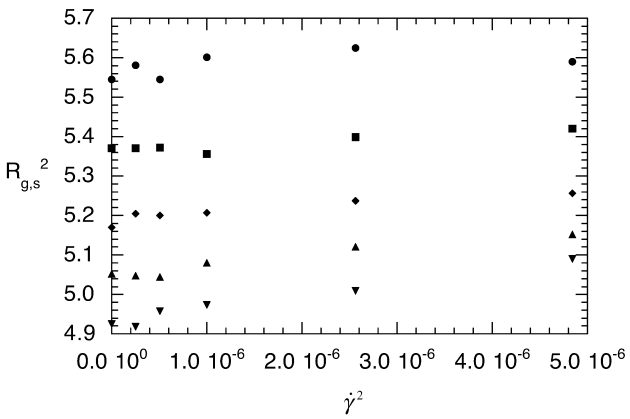

Fig. 1. Shear-dependent mean squared radius of gyration, $R_{g,s}^2$ versus squared strain rate $\dot{\gamma}^2$, for polymer concentrations $n_1 = 0.2$ (circles), $n_1 = 0.4$ (squares), $n_1 = 0.6$ (diamonds), $n_1 = 0.8$ (up triangles), and $n_1 = 1.0$ (down triangles). Error bars are approximately the same size as the plot symbols.

Table 2
Polymer molecule size and distortion: the mean squared radius of gyration, R_g^2, mean squared end-to-end distance R^2 and their ratio, and values of the gradient, a of $R_{g,s}^2$ versus $\dot{\gamma}^2$ shown in Fig. 1

n_1	$a \times 10^{-4}$	$\dot{\gamma} = 0.0$			$\dot{\gamma} = 0.0022$		
		R_g^2	R^2	R^2/R_g^2	R_g^2	R^2	R^2/R_g^2
0.2	1.2(4)	5.54(1)	36.4(2)	6.57(5)	5.59(1)	34.8(1)	6.22(3)
0.4	2.2(4)	5.33(1)	33(2)	6.2(4)	5.3(1)	33(1)	6.2(3)
0.6	3.0(4)	5.170(9)	33(1)	6.4(2)	5.26(1)	33(1)	6.3(2)
0.8	4.8(4)	5.051(8)	30(1)	5.9(2)	5.152(7)	31(1)	6.0(2)
1.0	6.6(4)	4.925(9)	29.5(9)	6.0(2)	5.09(1)	30.81(8)	6.05(3)

Numbers in brackets represent uncertainties.

The zero-shear-rate values of R_g^2 are plotted against concentration, n_1, in Fig. 2. The curve shown is a cubic polynomial fit. Extrapolating this fit back to $n_1 = 0.0$ gives a value for R_g^2 at zero shear rate and infinite dilution of $R_{g,0}^2 = 5.83(2)$. A similar analysis of the zero-shear values of R^2, the mean squared end-to-end distance of the polymer molecules (also shown in Table 2) produces the infinite dilution value $R_0^2 = 38(1)$. The resulting values of $R_{g,0} = 2.415(2)$ and $R_0 = 6.16(1)$ are similar to the values identified by Pierleoni and Ryckaert [30] for a 20-site bead-stiff-spring chain, simulated with Brownian Dynamics. They found that $R_{g,0} = 2.340(2)$ and $R_0 = 5.83(1)$. More obviously comparable results can be found in an earlier study by Pierleoni and Ryckaert [7] where molecular dynamics was used to simulate a single bead-rod model polymer, very similar (but not identical) to ours, which was subject to a WCA potential in an explicit Lennard–Jones solvent. While they reported $R_{g,0}$ and R_0 results for chain lengths of $N = 6, 9, 30$ only, the scaling of these values can be used to interpolate values of $R_{g,0} = 2.47$ and $R_0 = 6.06$ for an $N = 20$ chain, which are very close to our results.

The concentration dependence of the radius of gyration of long-chain polymers is often assumed to be negligible

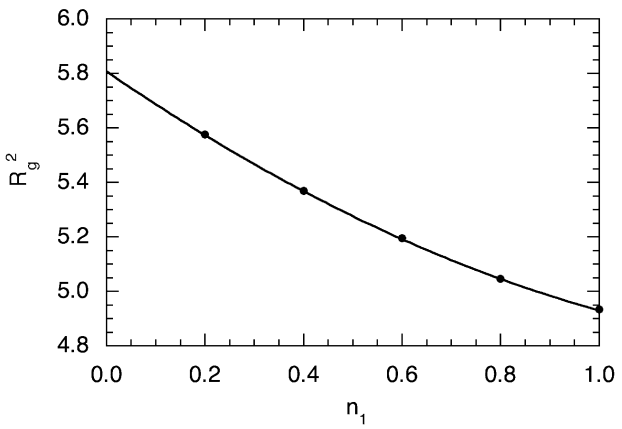

Fig. 2. Mean squared radius of gyration at equilibrium, R_g^2, versus polymer concentration, n_1. The solid line is a cubic polynomial fit to the data extrapolated to $n_1 = 0$ (infinite dilution). Error bars are smaller than plot symbols.

below the overlap concentration n_1^* and to vary due to the screening of excluded volume interactions in the semidilute concentration region. Our value of $R_{g,0}^2 = 5.83(2)$ can be used to calculate a value for n_1^* from

$$n_1^* = \frac{N}{\frac{4}{3}\pi R_g^3 \rho}, \tag{17}$$

which represents one of a number of plausible methods for evaluating n_1^*. (Note that the factor of ρ arises from our use of site fraction rather than mass concentration as our concentration unit.) This method assumes that crossover occurs when the average concentration of the solution is equal to the concentration within the domain (assumed to be spherical) of the polymer molecule using the radius of gyration at infinite dilution. Using this formulation, a value for n_1^* of 0.40(2) is obtained. An alternative that takes the change in the radius of gyration with concentration into account, is to perform the calculation using the radius of gyration in the melt. This gives an upper limit for n_1^* of 0.52. For comparison, an example of an alternative method for evaluating n_1^*, suggested by the experimental work of Nystrom and Roots [5], is to calculate it as the inverse of the intrinsic viscosity of the polymer ($n_1^* = [\eta]^{-1}$). Using the value $[\eta] = 4.0(4)$ (calculated below, in Section 3.2) we obtain the result $n_1^* = 0.25(3)$. These values for n_1^* differ considerably, but it should be understood that the onset of polymer overlap does not necessarily result in a sudden or obvious change in solution properties. Rather it can be regarded as a gradual change that occurs over a range of concentrations. We will take 0.40(2) as a reasonable estimate of the value of n_1^*, for this system.

Daoud et al. [9] used scaling arguments to predict a relationship between macromolecular size and solution concentration in the semidilute regime given by

$$R_g^2 \propto n_1^{\frac{2\nu-1}{3\nu-1}}, \tag{18}$$

where the excluded volume exponent, ν, is predicted by mean field theory to be equal to 0.6, and by renormalization group theory to be 0.588. Both of these values produce a value for the exponent of n_1 in Eq. (18) which is approximately $-1/4$. Experimental results for long chain polymer solutions are unable to distingush between the two theoretical values for the exponent of n_1 [31], but they do show that the slope of $\log(R_g^2)$ versus the log of concentration increases in magnitude with polymer concentration, exceeding $-1/4$ when the solution becomes concentrated [32]. The data shown in Fig. 3 demonstrate that the magnitude of the slope of $\log(R_g^2)$ versus $\log(n_1)$ increases with concentration for our system. However, while the general shape of this curve is similar to experimental results, the gradients of the data range from approximately $-1/20$ to $-1/10$. This difference reflects the differing conformational behaviour of the very short polymer chains used in this study and the long molecules used in experiments. Almost all of the solutions simulated in

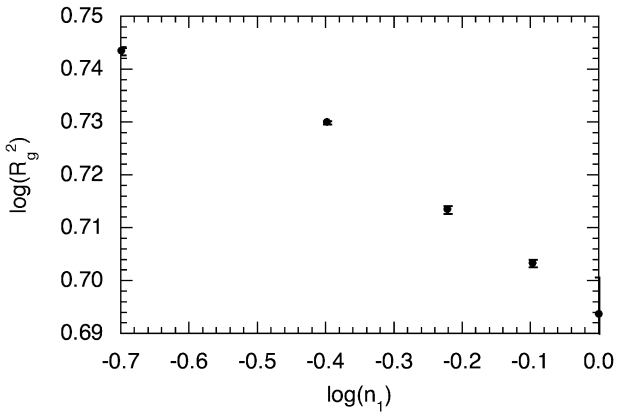

Fig. 3. Log of the mean square radius of gyration at equilibrium, $\log(R_g^2)$, versus log of polymer concentration, $\log(n_1)$.

this work have concentrations greater than the overlap concentration calculated above. The fact that we do not observe the predicted exponent for the change in polymer size with increasing concentration confirms that a semi-dilute region does not exist for our solutions of very short chain polymers. Considering that a semidilute region does not exist, we might expect the solution behaviour to cross over directly from the dilute to concentrated solution behaviour. In concentrated solutions, mean-field type behaviour might be expected. Mean field theory [4] predicts power-law behaviour for R_g^2 with an exponent of $-1/2$, which is still far from the values that we observe here. Therefore, neither the mean-field nor scaling theories predict the exponents that we observe.

We now examine the ratio of mean squared end-to-end distance R^2 to mean squared radius of gyration R_g^2 for the polymer molecules in each solution. Table 2 shows values of this ratio for solutions with and without shear. According to theory, the ratio R^2/R_g^2 is equal to 6, for sufficiently long, linear Gaussian chains and it increases to 6.302 for a long polymer in a good solvent [33]. The results in Table 2 show that the ratio is within uncertainties of the expected value of 6 for the melt ($n_1 = 1.0$), and that its value increases, as expected, as the concentration decreases. The value of the ratio in the limit of zero concentration obtained from a linear fit to the data is 6.6, which is considerably larger than the limiting value expected for long molecules, 6.302 [33]. This is consistent with the observation that the chain expansion is more pronounced near the centre of the molecule. For short polymers, this effect will be dominant, and a calculation that does not take into account the weakening of chain swelling for longer molecules gives a value of R^2/R_g^2 closer to 6.9 [34], indicating that a higher value than 6.302 might be expected for short chains.

The distortion of the polymer molecules under shear is demonstrated by the $\dot{\gamma} = 0.0022$ results in Table 2. Here, all values of R^2/R_g^2 are less than their corresponding equilibrium values.

These variations are exhibited in more detail in the site statistics plots (Figs. 4–7) where the logarithm of the ensemble averaged rms distance between polymer sites i and j, given by $\log\langle R_{ij}^2\rangle^{1/2}$, is plotted against the logarithm of the number of bonds between the two sites, $\log|j-i|$. A solid line of gradient 0.6 is also included to illustrate the degree to which each system adheres to the prediction that $\langle R_{ij}^2\rangle^{1/2} \propto |j-i|^{\nu}$ with $\nu = 0.6$ for a polymer in a good solvent, and thus demonstrate when excluded volume effects are dominant.

Figs. 4 and 5 show the site statistics at equilibrium for polymer concentrations of $n_1 = 0.4$ and 0.8, respectively. Clearly, the results for $n_1 = 0.4$ conform closely to the $\nu = 0.6$ gradient, strongly exhibiting an excluded volume effect, while the site statistics for $n_1 = 0.8$ deviate significantly from this behaviour. This is further elucidated in Table 3.

For comparison, plots of these results for the maximum shear rate, $\dot{\gamma} = 0.0022$, are shown in Figs. 6 and 7. There is minimal difference in site statistics between Figs. 4 and 6 where $n_1 = 0.4$ (just above n_1^*) and the molecules are already swollen before shear is applied. Under shear, the lower concentration solutions are only slightly affected, with the greater flexibility of the chain ends leading to some increased deformation at the high $|j-i|$-values. By contrast, the obvious difference between Figs. 5 and 7, where the solution has a concentration $n_1 = 0.8$, indicates that the polymer molecules are randomly coiled at equilibrium, and that even relatively weak shear flow can deform them. The conformity of the Fig. 7 data with the line of gradient 0.6 is probably coincidental. The $\langle R_{ij}^2\rangle^{1/2}$ distances are spherically averaged, so the increase in their magnitudes with the application of shear reflects a stretching of the molecules in one direction, rather than enhancement of the excluded volume effect. These results confirm the conclusions drawn earlier from Fig. 1, where it was observed that polymer molecules in concentrated solutions are unperturbed at equilibrium and undergo more expansion under shear than do identical molecules in more dilute systems. Table 3 provides a quantitative measure of these observations by listing the gradients of linear fits to the

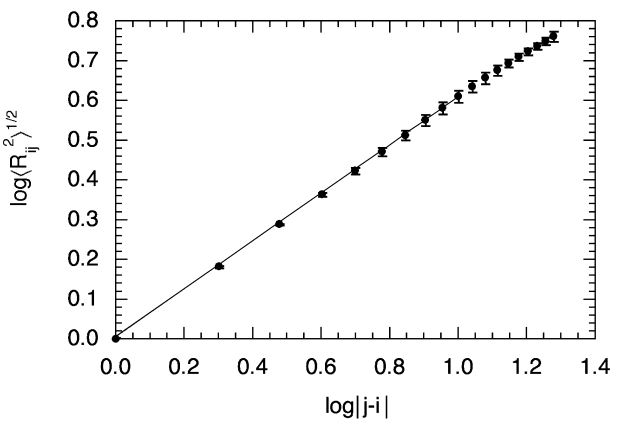

Fig. 4. Site statistics for $n_1 = 0.4$ at equilibrium. The solid line indicates a gradient of 0.6.

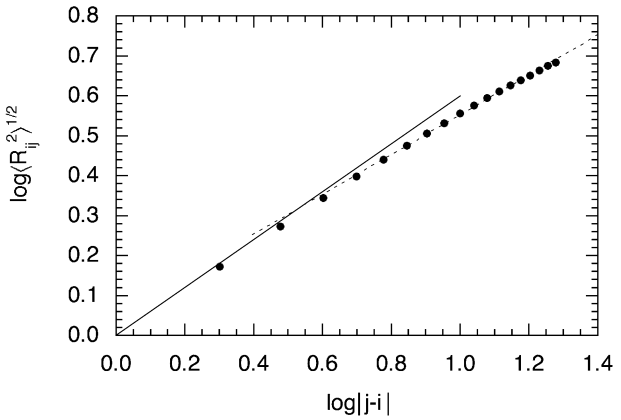

Fig. 5. Site statistics for $n_1 = 0.8$ at equilibrium. The solid line indicates a gradient of 0.6 and the dashed line indicates a gradient of 0.5.

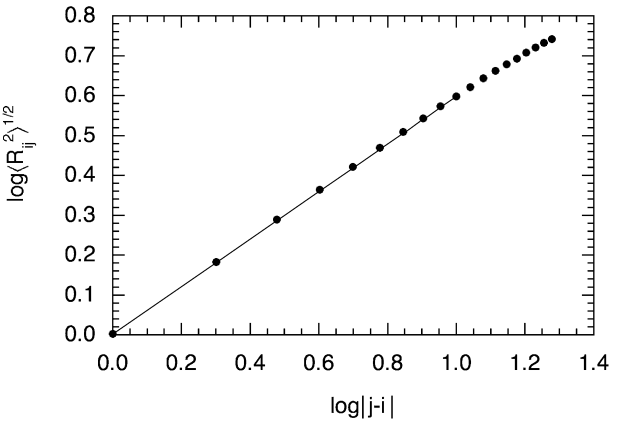

Fig. 7. Site statistics for $n_1 = 0.8$ at $\dot{\gamma} = 0.0022$. The solid line indicates a gradient of 0.6.

$\log\langle R_{ij}^2\rangle^{1/2}$ versus $\log|j-i|$ data. This table lists the gradients of $\log\langle R_{ij}^2\rangle^{1/2}$ versus $\log|j-i|$ data calculated for the whole length of the 20-site chains ($|j-i|_{\max} = 19$), and for all polymer sites except for one ($|j-i|_{\max} = 17$) and two ($|j-i|_{\max} = 15$) at either end of the chains. Included in this table, but not illustrated graphically, are the data for $n_1 = 0.6$ which fall, as one would expect, between the values for $n_1 = 0.4$ and 0.8. Also included but not illustrated is an example of the gradient of $\log\langle R_{ij}^2\rangle^{1/2}$ versus $\log|j-i|$ for $n_1 = 0.4$ where only the sites in approximately the middle third of the chains are included ($|j-i|_{\max} = 7$).

As implied by Fig. 4, the gradients of all $n_1 = 0.4$ results are within errors of $\nu = 0.6$, the expected value for a dilute solution of a polymer in a good solvent. Interestingly, while the results for $n_1 = 0.6$ and $n_1 = 0.8$ produce gradients which exceed $\nu = 0.5$, the gradient 0.5 forms a tangent to the results when the first few $|j-i|$ values are ignored (as indicated by dotted line in Fig. 5). This confirms that the chain statistics for $n_1 = 0.6$, 0.8 and higher concentrations tend towards random walk behaviour, like a dilute solution of polymer in a theta solvent, as predicted by Flory.

The conformational data given above can be used to calculate the Kuhn length, b_K, the characteristic ratio, and

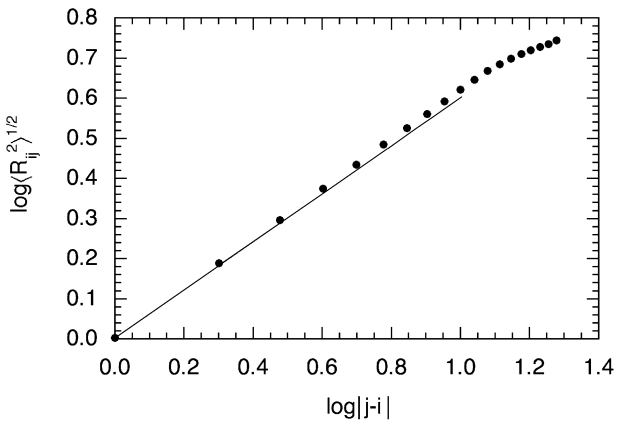

Fig. 6. Site statistics for $n_1 = 0.4$ at $\dot{\gamma} = 0.0022$. The solid line indicates a gradient of 0.6.

the number of bonds per Kuhn segment for our model polymer. These quantities are defined for unperturbed conditions. In our simulations, we do not have a theta solvent, but unperturbed conditions are achieved in the melt. At zero shear rate, we can use the rms end-to-end distance and the contour length of our model polymer, $L = (N-1)l$, to obtain $b_K = R^2/L = 1.55$ and the number of Kuhn segments per molecule, $N_K = L/b_K = 12.2$. This corresponds to a characteristic ratio of $C_\infty = R^2/l^2(N-1) = 1.55$, indicating that this is a very flexible model chain. This value can be compared with the value of 1.79 obtained for the FENE chain model used by Kröger and Hess [37].

The value of N_K that we have obtained also makes it possible to estimate the molar mass of a polyethylene molecule with an equivalent number of Kuhn steps to our model polymer. Using a value of the characteristic ratio of polyethylene in the melt at 440 K of $C_\infty = 7.2$ [38] and the contour length $L = l(N-1)g$ where g is a geometrical factor equal to 0.83 for polyethylene, we find that 12.2 Kuhn segments corresponds to polyethylene of around 128 monomers, or a molar mass of 1800 g/mol.

With the value of the Kuhn length of 1.55 and the rms end-to-end distance $R = 6.16$ that we have obtained, we can now establish that there can be no length scale ξ satisfying the condition $b_K \ll \xi \ll R$ in our solutions. This makes it clear that no semidilute region exists for the short polymer chains studied here. Only two concentration regions, dilute and concentrated, exist for these solutions.

Table 3
Gradients of linear fits to $\log\langle R_{ij}^2\rangle^{1/2}$ versus $\log|j-i|$ at equilibrium

n_1	$\lvert j-i\rvert_{\max} = 7$	$\lvert j-i\rvert_{\max} = 15$	$\lvert j-i\rvert_{\max} = 17$	$\lvert j-i\rvert_{\max} = 19$
0.4	0.63(2)	0.608(4)	0.604(4)	0.601(4)
0.6		0.57(1)	0.56(2)	0.56(1)
0.8		0.54(1)	0.54(2)	0.53(2)

3.2. Viscometric functions

The most significant results of this study come from the analysis of the viscometric functions. We are unaware of any other published results for the viscosity and first and second normal stress coefficients, obtained from simulations of polymer solutions, covering the entire polymer concentration range.

Fig. 8 shows the relationship between shear viscosity, η_s, and $\dot{\gamma}^2$ for each of the six different polymer solution concentrations simulated. At these very low strain rates, the strain-rate dependence of the viscosity is very weak over the entire concentration range, though it becomes marginally stronger at high polymer concentrations. The monatomic solvent is Newtonian at these strain rates. Matin, Daivis and Todd [24] have found that for an atomic fluid identical to the one simulated here, the power-law shear thinning regime does not begin until $\dot{\gamma}^2 = 0.073$. For all concentrations studied here, the low strain rate $\dot{\gamma}^2$-dependence of η_s is linear. Consequently, the zero strain rate viscosity, η, can be easily obtained from the intercept of a linear fit to the η_s versus $\dot{\gamma}^2$ data of the form

$$\eta_s(\dot{\gamma}) = \eta + b_1\dot{\gamma}^2. \tag{19}$$

The zero-shear rate viscosities and slopes are recorded in Table 4.

The first and second normal stress differences, N_1 and N_2, as defined in Section 2.3, result from forces opposing any flow-induced anisotropy in the system. Results for these values, plotted against $\dot{\gamma}^2$, for each of the different polymer concentrations simulated, are shown in Figs. 9 and 10. The data for N_2 are noisy, close to zero and not indicative of any clear trend. Such ambiguous results are common when analyses of N_2 are attempted, especially at low strain rates. By comparison, trends in the N_1 data are relatively clear. The relationship between N_1 and $\dot{\gamma}^2$ appears to be linear for each of the different polymer concentrations, indicating that the first normal stress coefficient is independent of shear rate within the range investigated (Fig. 9).

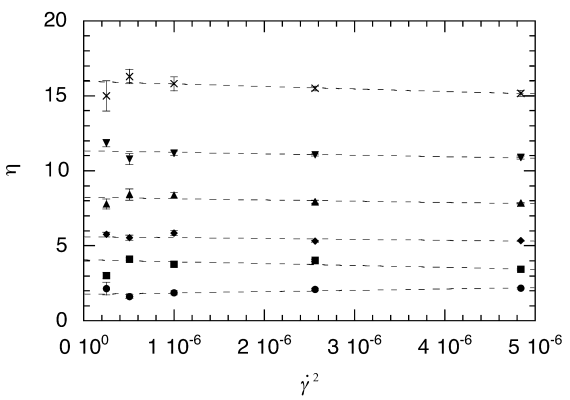

Fig. 8. Shear viscosity η_s versus squared strain rate ($\dot{\gamma}^2$), for polymer concentrations $n_1 = 0.0$ (circles), $n_1 = 0.2$ (squares), $n_1 = 0.4$ (diamonds), $n_1 = 0.6$ (up triangles), $n_1 = 0.8$ (down triangles), and $n_1 = 1.0$ (crosses).

Table 4
Viscometric properties. Results in square brackets are for a 5120-site system, all others are for 10,000-site systems

n_1	η	b_1	$\Psi_{1,0}/10^2$
0.0	1.8(1)	90(30)	−0.3(8)
0.2	4.03(7)	$-1.3(2)\times10^5$	−0.6(4)
[0.2]	[3.4(3)]		
0.4	5.60(9)	$-0.6(2)\times10^5$	5.5(9)
0.6	8.2(1)	$-0.8(3)\times10^5$	7.8(7)
0.8	11.32(1)	$-1.0(4)\times10^5$	15.0(8)
1.0	15.9(3)	$-1.7(8)\times10^5$	33(2)

It is evident from Table 4 and Fig. 8 that the zero shear rate viscosity increases with increasing polymer concentration. A combination of scaling theory with the reptation model gives the simple prediction that the viscosity varies as $\eta \propto N^3 n_1^{15/4}$ for very long molecules [4]. This is clearly not applicable to the short molecules studied here, which are far below the length required for the onset of entanglement coupling. If we use the N dependence predicted by the Rouse and Zimm models for unentangled polymers instead of the repetition prediction, we obtain $\eta \propto N n_1^{5/4}$. This result might be expected to hold for a semidilute solution of molecules with molar masses below the value required for the onset of entanglement coupling. Our data for $\log(\eta)$ versus $\log(n_1)$ are plotted in Fig. 12. Although a gradient of 5/4 is tangent to the results, there is no evidence for a power-law region, and the data are better described by the simple quadratic polynomial fit shown in Fig. 11.

The zero shear-rate viscosities are also useful in the evaluation of $[\eta]$, the intrinsic viscosity, which is a property of a given polymer-solvent pair. The intrinsic viscosity is defined by the zero-concentration limit of η_{sp}/n_1 where the specific viscosity, η_{sp}, is given by

$$\eta_{sp} = \frac{\eta - \eta_0}{\eta_0}, \tag{20}$$

η_0 is the zero shear rate viscosity of the solvent and η is the zero shear rate viscosity of each solution. Table 4 shows

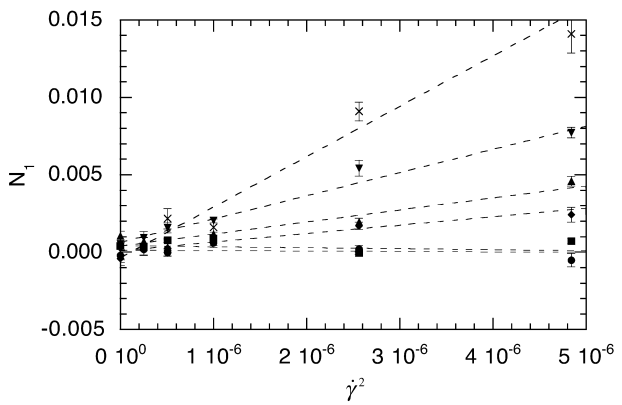

Fig. 9. First normal stress differences N_1 versus squared strain rate ($\dot{\gamma}^2$), for polymer concentrations $n_1 = 0.0$ (circles), $n_1 = 0.2$ (squares), $n_1 = 0.4$ (diamonds), $n_1 = 0.6$ (up triangles), $n_1 = 0.8$ (down triangles), and $n_1 = 1.0$ (crosses).

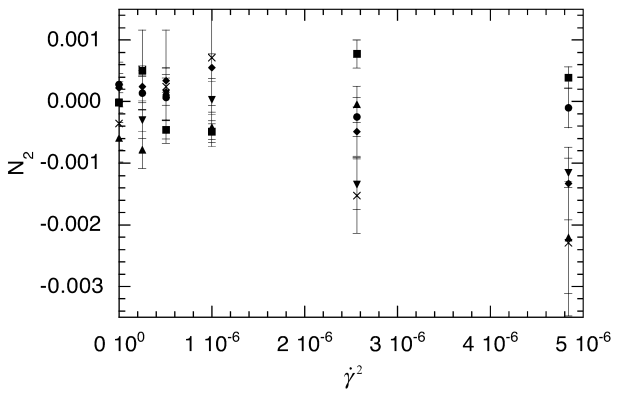

Fig. 10. Second normal stress difference N_2 versus squared strain rate ($\dot{\gamma}^2$), for polymer concentrations $n_1 = 0.0$ (circles), $n_1 = 0.2$ (squares), $n_1 = 0.4$ (diamonds), $n_1 = 0.6$ (up triangles), $n_1 = 0.8$ (down triangles), and $n_1 = 1.0$ (crosses).

the zero shear-rate viscosity and other results for an $n_1 = 0.2$ solution of approximately half the volume of the other systems simulated in this work. This result is included to show the agreement between results for systems with very different volumes, demonstrating the absence of artifacts related to the use of periodic boundary conditions.

The equation for the second-order polynomial fit to the data shown in Fig. 11, excluding the $n_1 = 1.0$ value, is given by

$$\eta = 1.9(1) + 7.7(3)n_1 + 4.9(1)n_1^2. \tag{21}$$

The Huggins equation links concentration and intrinsic viscosity, according to

$$\eta = \eta_0(1 + n_1[\eta] + k_H n_1^2[\eta]^2 + \cdots)$$
$$= \eta_0 + \eta_0[\eta]n_1 + \eta_0 k_H[\eta]^2 n_1^2 + \cdots \tag{22}$$

Equating coefficients of Eqs. (21) and (22) allows us to evaluate the intrinsic viscosity and Huggins constant, k_H, for this system. We obtain a value of $[\eta] = 4.0(4)$ for the intrinsic viscosity and $k_H = 0.16(4)$ for the Huggins constant where the concentration in expressed in terms of

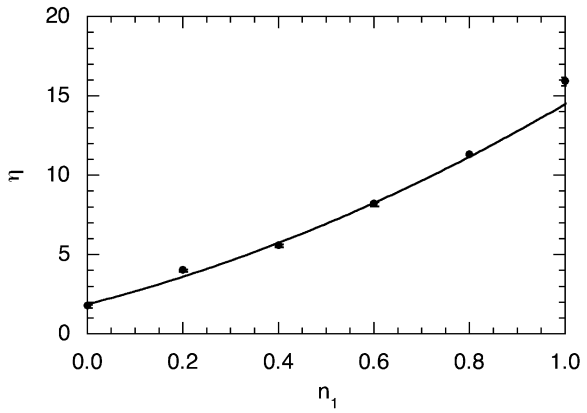

Fig. 11. Zero-shear viscosity η versus polymer concentration n_1. Linear plot showing second-order polynomial fit to data.

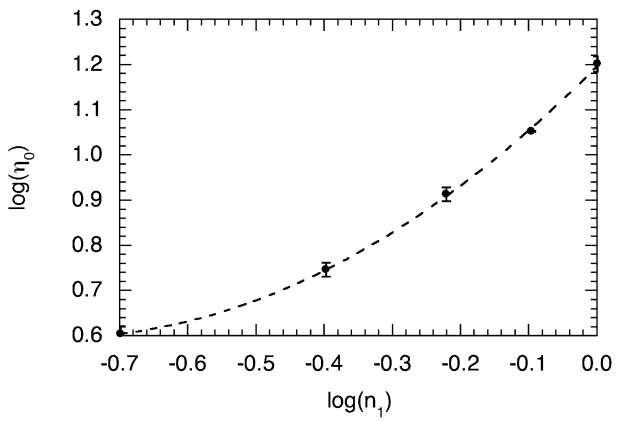

Fig. 12. Log of zero shear viscosity $\log(\eta)$ versus log of polymer concentration $\log(n_1)$.

site fraction. If the concentration is expressed in terms of mass/volume, the value of the intrinsic viscosity becomes $[\eta] = 4.8$ and k_H is unchanged.

To circumvent the difficulty of comparing our intrinsic viscosity result with the results of experimental measurements of long-chain systems, we calculate the dimensionless quantity Φ, the Flory–Fox parameter, defined by

$$\Phi = \frac{N_A U_{\eta/s}}{6^{\frac{3}{2}}}. \tag{23}$$

Here, N_A is Avogadro's number and $U_{\eta/s}$ is defined in reduced units by [3]

$$U_{\eta/s} = \frac{M[\eta]}{R_g^3}. \tag{24}$$

Φ is a useful parameter for comparing experimental results for different solutions. When this parameter is evaluated using our calculated values for $[\eta]$ (after conversion to mass/volume concentration units) and $R_{g,0}^2$, it produces the result $\Phi = 2.79(5) \times 10^{23}$. This falls below the theoretical value, $\Phi = 2.84 \times 10^{23}$, calculated using the Zimm model by Osaki [34], and the earlier Pyun–Fixman [35] value of $\Phi = 2.68 \times 10^{23}$. A more recent theoretical calculation by Oono [3] gives a value of 2.36×10^{23}. Our result is also close to the range of experimental values for Φ quoted by Krigbaum and Carpenter [36]. They summarise results from experimental studies of solutions of polystyrene, polyisobutylene and polysilicons at various (high) molecular weights, giving values of Φ which, when the measured vaues are converted into compatible units, fall between 2.5×10^{23} and 2.8×10^{23}. Note that the theoretical values that we compare with are calculated for theta conditions. For a polymer in a good solvent, the value of Φ is expected to decrease with increasing solvent quality and molar mass [4].

The fact that our value of k_H falls below 0.3 confirms that the solvent we are simulating is very good. It is also interesting to note that while the quadratic fit to the specific viscosity data is expected to agree only in the dilute region,

where the Huggins equation is known to apply, Fig. 11 shows that for this system, Huggins-like behaviour persists over a much broader concentration range. This is consistent with the concentration dependence of the radius of gyration, which also displays relatively simple polynomial behaviour.

4. Conclusion

We have studied the concentration dependence of the conformational and rheological properties of WCA-potential polymer chains with $N = 20$, in an explicitly modelled solvent, by non-equilibrium molecular dynamics. Although polymer conformation and viscosity in an atomic solvent have been studied before, the work reported here appears to be unique among computer simulation studies in examining the variation of these properties across the entire concentration range.

The overlap concentration (expressed in terms of the polymer site fraction) for this particular system is estimated as falling within the range $0.40 \leq n_1^* < 0.52$. Solutions with lower concentrations are shown to clearly experience a strong excluded volume effect, with the end to end distance between beads along the chain depending on the number of intervening bonds with an exponent of $\nu = 0.6$. As the concentration is raised, R_g decreases, as expected. In the melt, the chain statistics are well described by the random walk model and the molecules can be regarded as unperturbed. These features are typical of the behaviour of a polymer in a good solvent. However, the concentration dependence of the radius of gyration does not follow the power laws predicted by scaling or mean-field theories, and the usual explanation for the change in molecular size with concentration in terms of screening of the excluded volume interaction does not seem to apply, presumably because these molecules are so short.

In the presence of a weak shear field, the molecules are distorted, and R_g increases linearly with $\dot{\gamma}^2$, the rate of increase becoming larger for the high concentration systems. It is postulated that the shear field has a weaker effect on the dilute solutions because the molecules are already expanded in dilute solutions of polymers in a good solvent.

By using very low values for $\dot{\gamma}$ we have been able to observe a regime in which the more concentrated solutions are slightly shear thinning, while the solvent is Newtonian. The viscosity increases linearly with $\dot{\gamma}^2$ over the range of shear rates investigated, allowing us to obtain precise values of the zero shear rate viscosity for all concentrations. The zero shear rate viscosity, η, increases with polymer concentration, and is again well described by a polynomial, rather than a power law dependence on concentration. The value of the intrinsic viscosity of this polymer is found to be $[\eta] = 4.0(4)$. This value is used with the radius of gyration to calculate the Flory–Fox parameter for this system, giving $\Phi = 2.79(5) \times 10^{23}$, which is close to the theoretically calculated and experimentally measured values for much longer chains than those studied here. The Huggins coefficient is also obtained, giving the value $k_H = 0.16(4)$.

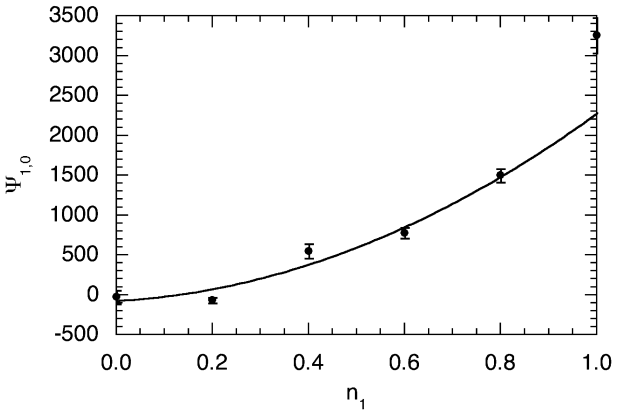

Fig. 13. Concentration dependence of the first normal stress coefficient.

We have also computed the value of the first normal stress coefficient $\Psi_{1,0}$, as a function of concentration (Fig. 13). We find that $\Psi_{1,0}$ increases strongly with concentration, once again following a quadratic concentration dependence over most of the concentration range.

Taken together, these results and our previous results for the rheological properties of short chain polymer melts, indicate that in dilute solutions and in the melt many manifestations of typical polymer behaviour are observed for the short chains studied here. The agreement between our value of the Flory–Fox constant and theoretical values, and the exponents found in the chain conformational data for the dilute solutions imply that the usual description in terms of the Zimm model and the self avoiding walk are appropriate. The decrease in the radius of gyration, the increase in the viscosity and the random walk behaviour in the melt are also consistent with the typical polymer behaviour. However, the concentration dependence of R_g and η_s is not quantitatively described by scaling or mean field theory, both of which assume that screening is the main mechanism governing the concentration dependence of these quantities above the overlap concentration. The overlap concentration is so high for these solutions that a semidilute region does not exist. Instead, we observe a large concentration regime in which 'virial' (polynomial) behaviour is observed. These observations indicate that a mechanism other than screening is probably responsible for the concentration dependence of R_g in very short chain polymer solutions.

Acknowledgements

This work was supported by the Cooperative Research Centre for MicroTechnology and through an Expertise Grant from the Victorian Partnership for Advanced Computing. We would like to thank the CSIRO/Bureau of

Meteorology High Performance Computing and Communications Centre and the Australian and Victorian Partnerships for Advanced Computing for generous allocations of computer time.

References

[1] de Gennes P-G. Scaling concepts in polymer physics. Ithaca: Cornell University Press; 1979.
[2] des Cloizeaux J, Jannink G. Polymers in solution: their modelling and structure. Oxford: Clarendon Press; 1990.
[3] Oono Y. Adv Chem Phys 1985;61:301.
[4] Doi M, Edwards SF. The theory of polymer dynamics. Oxford: Clarendon Press; 1986.
[5] Roots J, Nystrom B. Polymer 1979;20:148.
[6] Dunweg B, Kremer K. Phys Rev Lett 1991;66:2996.
[7] Pierleoni C, Ryckaert J-P. Phys Rev Lett 1991;66:2992.
[8] Ahlrichs P, Everaers R, Dunweg B. Phys Rev E 2001;64(040501): 1–4.
[9] Daoud M, Cotton JP, Farnoux G, Jannink G, Sarma G, Benoit H, Duplessix R, Picot C, de Gennes PG. Macromolecules 1975;8:804.
[10] Weeks JD, Chandler D, Andersen HC. J Chem Phys 1971;54:5237.
[11] Evans DJ, Morriss GP. Statistical mechanics of nonequilibrium liquids. London: Academic Press; 1990.
[12] Sarman SS, Evans DJ, Cummings PT. Phys Rep 1998;1:92.
[13] Edberg R, Evans DJ, Morriss GP. J Chem Phys 1986;84:6933.
[14] Edberg R, Morriss GP, Evans DJ. J Chem Phys 1987;86:4555.
[15] Morriss GP, Evans DJ. Comput Phys Commun 1991;62:267.
[16] Travis KP, Daivis PJ, Evans DJ. J Chem Phys 1995;103:1109.
[17] Travis KP, Daivis PJ, Evans DJ. J Chem Phys 1995;103:10638. Erratum: J Chem Phys 1996;105:3893.
[18] Travis KP, Evans DJ. Mol Simul 1996;17:157.
[19] Padilla P, Toxvaerd S. J Chem Phys 1996;104:5956.
[20] Bair S, McCabe C, Cummings PT. Phys Rev Lett 2002;88(058302): 1–4.
[21] Bird RB, Curtiss CF, Armstrong RC, Hassager O, Dynamics of polymeric liquids, vol. 2. New York: Wiley; 1987.
[22] Todd BD, Daivis PJ. Phys Rev Lett 1998;81:1118.
[23] Todd BD, Daivis PJ. Comput Phys Commun 1999;117:191.
[24] Erratum:Matin ML, Daivis PJ, Todd BD. J Chem Phys 2000;113: 9122. Matin ML, Daivis PJ, Todd BD. J Chem Phys 2001;115:5338.
[25] Matin ML, Daivis PJ, Todd BD. Comput Phys Commun 2003;151:35.
[26] Daivis PJ, Matin ML, Todd BD. J Non-Newtonian Fluid Mech 2003; 111:1.
[27] Matin ML. Molecular simulation of polymer rheology. PhD Thesis. Applied Physics, RMIT University, Melbourne; 2001.
[28] Zimm BH, Stockmayer WH. J Chem Phys 1949;17:1301.
[29] Flory PJ. Principles of polymer chemistry. London: Cornell University Press; 1971.
[30] Pierleoni C, Ryckaert J-P. J Chem Phys 2000;113:5545.
[31] Richards RW, Davidson NS. Macromolecules 1986;19:1381.
[32] Adachi K, Imanishi Y, Shinkado T, Kotaka T. Macromolecules 1989; 22:2391.
[33] Jannink G, des Cloizeaux J. J Phys: Condens Matter 1990;2:1.
[34] Osaki K. Macromolecules 1972;5:141.
[35] Pyun CW, Fixman M. J Chem Phys 1965;42:3838.
[36] Krigbaum WR, Carpenter DK. J Phys Chem 1955;59:1166.
[37] Kröger M, Hess S. Phys Rev Lett 2000;85:1128.
[38] Fetters LJ, Graessley WW, Krishnamoorti R, Lohse DJ. Macromolecules 1997;30:4973.